AGU ADVANCING EARTH AND SPACE SCIENCES

Geophysical Research Letters

RESEARCH LETTER
10.1029/2025GL116804

Probing Jupiter's Atmosphere Through Juno Radio Occultations: Analysis of the Atmospheric Thermal Structure

Maria Smirnova[1], Eli Galanti[1], Andrea Caruso[2], Leigh N. Fletcher[3], Dustin R. Buccino[4], Luis Gomez Casajus[2], William B. Hubbard[5], Glenn S. Orton[4], Marzia Parisi[4], Ryan S. Park[4], Marco Zannoni[2], Paul G. Steffes[6], Steven M. Levin[7], Scott J. Bolton[7], Paolo Tortora[2], and Yohai Kaspi[1]

[1]Department of Earth and Planetary Sciences, Weizmann Institute of Science, Rehovot, Israel, [2]Department of Industrial Engineering, University of Bologna, Forlì, Italy, [3]School of Physics and Astronomy, University of Leicester, Leicester, UK, [4]Jet Propulsion Laboratory, California Institute of Technology, Pasadena, CA, USA, [5]Lunar and Planetary Laboratory, University of Arizona, Tucson, AZ, USA, [6]School of Electrical and Computer Engineering, Georgia Institute of Technology, Atlanta, GA, USA, [7]Southwest Research Institute, San Antonio, TX, USA

Abstract The upper layers of Jupiter's atmosphere, offering critical insights into the planet's deeper structure, are accessible through radio occultation experiments. Since July 2023, NASA's Juno extended mission has provided the first high-resolution radio occultation measurements since the Voyager era, probing the thermal structure and composition down to approximately 0.5 bar. We use these measurements to study Jupiter's latitudinally dependent vertical thermal structure. We observe cooler stratospheric and warmer tropospheric temperatures at the equatorial region compared to mid- and high-latitudes, and temporal variations in the North Equatorial Belt's thermal structure on a time scale of a few months. These observations align with archival mid-infrared data from Cassini's CIRS and current ground-based Texas Echelon Cross Echelle Spectrograph observations, as well as previous studies based on Voyager radio occultations and the Galileo probe, offering an enhanced view of Jupiter's lower stratosphere and upper troposphere thermal structure.

Plain Language Summary Jupiter's troposphere and lower stratosphere provide crucial insights into the planet's deeper structure, accessible through both direct sampling and remote sensing. Radio occultation experiments offer a unique way to study the thermal structure and composition of these layers at high vertical resolution, similar to what a descending probe would reveal. However, such measurements at Jupiter have been rare. Since July 2023, NASA's Juno mission has expanded this capability, delivering the first series of high-resolution radio occultation measurements since the Voyager mission four decades ago. By measuring how radio signals bend through the atmosphere, these occultations reveal detailed vertical temperature profiles down to the 0.5-bar level. We also compare our results with previous thermal analysis from Cassini's CIRS instrument and recent Texas Echelon Cross Echelle Spectrograph (TEXES) observations from the ground. We see clear variations in the North Equatorial Belt, where the upper stratosphere is cooler and the troposphere is warmer than in areas farther from the equator. This matches what has been seen in previous mid-infrared observations like CIRS and TEXES.

Key Points:

- Juno's radio occultations deliver latitudinally-dependent atmospheric profiles of Jupiter, the first since Voyager in the 1970s
- We show recent evidence for a cooler stratosphere and warmer troposphere at 15N compared to high latitudes and strong temporal variability
- Our results are corroborated by Cassini's CIRS and TEXES measurements taken contemporaneously, and by previous radio occultations

Supporting Information:

Supporting Information may be found in the online version of this article.

Correspondence to:

M. Smirnova and Y. Kaspi,
maria.smirnova@weizmann.ac.il;
yohai.kaspi@weizmann.ac.il

Citation:

Smirnova, M., Galanti, E., Caruso, A., Fletcher, L. N., Buccino, D. R., Gomez Casajus, L., et al. (2025). Probing Jupiter's atmosphere through Juno radio occultations: Analysis of the atmospheric thermal structure. *Geophysical Research Letters*, *52*, e2025GL116804. https://doi.org/10.1029/2025GL116804

Received 27 OCT 2024
Accepted 24 OCT 2025

1. Introduction

Jupiter's troposphere and lower stratosphere (1 bar–1 mbar) play a key role in mediating energy exchange between atmospheric levels, yet their detailed structure, composition, and dynamics have remained challenging to resolve due to limited high-resolution observations. Jupiter's atmosphere is generally divided into the lower troposphere (below the 500-mbar level), the upper troposphere (100–500 mbar), and the lower stratosphere (1–100 mbar). At the cloud tops, zonal wind fields observed since the Voyager era reveal alternating prograde and retrograde jets that serve as key indicators of atmospheric circulation (Ingersoll & Cuong, 1981; Kaspi et al., 2018, 2023; Limaye et al., 1982; Sánchez-Lavega et al., 2019). Above the 300-mbar level, the atmosphere becomes increasingly stratified and below, it transitions toward a dry adiabat near 1 bar (Fletcher et al., 2023). In this radiatively controlled regime, solar energy is absorbed in methane bands while internal heat continues to rise from below, creating a delicate balance that governs the temperature structure and influences the transport of heat and trace gases (Conrath et al., 1981; Simon-Miller et al., 2004). The stratosphere is characterized by increasing

temperatures with altitude, primarily due to near-infrared solar absorption by methane, with cooling dominated by emissions from methane, ethane, and acetylene. A sharp temperature rise near the upper stratosphere has been attributed to hydrocarbon separation and declining radiative cooling efficiency (Lindal et al., 1981). However, the vertical resolution and temporal coverage of past measurements have been insufficient to fully resolve these structures or assess their variability across latitude and time (Antuñano et al., 2018; Guerlet et al., 2020; Orton et al., 2023).

Jupiter's neutral atmosphere has been characterized in more detail over time. Initial thermal data came from ground-based observations (Fletcher, Kaspi et al., 2020; Fletcher, Orton et al., 2020; Orton et al., 1998), with early improvements from Pioneer 10 and 11 (Hubbard et al., 1975; Kliore et al., 1976). Voyager 1 and 2 marked a major advance, achieving profiles with vertical resolutions of about 5 km (Conrath et al., 1998) and providing detailed cloud and spectral data (Simon-Miller et al., 2006). The Galileo probe offered deeper atmospheric insights (Seiff et al., 1998) but the Galileo orbiter itself lacked occultation data from the lower stratosphere and upper troposphere due to antenna issues (Hinson et al., 1997). Cassini's 2000 flyby, using the CIRS instrument, enabled more detailed atmospheric mapping (Flasar et al., 2004; Fletcher et al., 2016; Simon-Miller et al., 2006). While infrared mapping from ground-based telescopes is now routine, remote sensing still faces challenges related to vertical resolution, calibration, and spectral inversion (Fletcher et al., 2016).

A crucial high-resolution technique for probing the atmosphere above the 1-bar level, that avoids these limitations, is radio occultation (RO). This method was first employed at Jupiter by the Pioneer (Ingersoll, 1976; Kliore et al., 1976) and Voyager (Allison, 1990; Lindal et al., 1981) missions. Despite their effectiveness, only five soundings of Jupiter's atmosphere were conducted in past missions, underscoring the rarity of such experiments. Recent reanalysis of Voyager occultations by Gupta et al. (2022) has incorporated more advanced knowledge of atmospheric composition, refining these observations. Radio occultations remain a powerful tool for probing Jupiter's atmosphere at high resolution, and are also a key part of the JUICE mission in the 2030s (Fletcher et al., 2023).

For the first time in over four decades, Jupiter's troposphere and lower stratosphere are probed with unprecedented precision using radio occultations. NASA's Juno mission, in orbit since 2016 (Bolton, Adriani, et al., 2017), now enables the first retrieval of high-resolution vertical temperature profiles of Jupiter's upper troposphere and lower stratosphere via RO experiments (Bolton, Lunine, et al., 2017). These observations became possible with the mission's extension in 2021, which introduced a modified polar orbit allowing periodic ingress and egress occultations as viewed from Earth. Between 2023 and 2025, these events provide repeated opportunities to probe Jupiter's atmosphere across a range of latitudes and longitudes. Our study focuses on the neutral atmosphere (ionospheric measurements are discussed in Coffin et al. (2025)), using Juno's occultation data to directly quantify previously inferred thermal structures and assess their spatial and temporal variability. In addition, Juno has performed occultation experiments of several Jovian moons (Buccino et al., 2022; Parisi et al., 2023), though these are not addressed here.

This study presents the first year of Juno's radio occultations, conducted between July 2023 and July 2024, focusing on the numerous high-quality measurements in Jupiter's Northern Hemisphere. Figure 1 shows the locations of these ingress and egress occultations. While the initial PJ-53, PJ-54, and PJ-60 occultations were grazing experiments, resulting in either shallow atmospheric coverage or degraded signal quality, particularly in the Ka band due to increased horizontal variability, deeper and more stable occultations began in May 2024, offering more comprehensive insights. We analyze these radio occultations to investigate the thermal structure and variability of Jupiter's lower stratosphere and upper troposphere, comparing our findings with previous data from Cassini's CIRS and recent TEXES ground-based observations, conducted in conjunction with the Juno mission (Fletcher et al., 2016; Sinclair et al., 2017).

2. Data Analysis

2.1. The Radio Occultation Experiments

During RO experiments, the Juno spacecraft transmits radio signals at multiple frequencies, specifically in the X-band (8.4 GHz) and Ka-band (32 GHz), which are received by the Deep Space Network (DSN) stations as the spacecraft passes behind planetary bodies. Since radio occultations were not initially planned as part of the mission's experiments, Juno does not carry an ultra-stable oscillator onboard (Buccino et al., 2023).

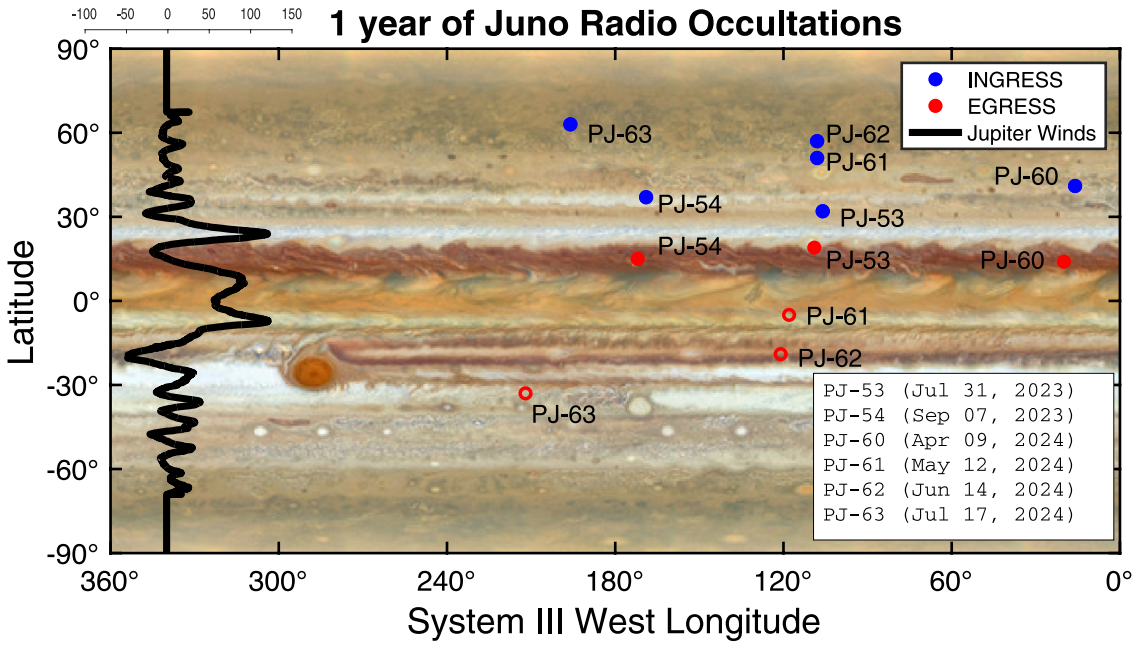

Figure 1. Distribution of the first year of the Juno ingress (blue) and egress (red) radio occultations (PJ53-PJ63). Profiles represented in Figure 2 are indicated with full circles. Background shows a map of the clouds of Jupiter from the Hubble telescope from 2019 (Simon et al., 2015). Also shown is the strength of the zonal winds in ms^{-1} from cloud tracking between measured between 2009 and 2016 (black line, from Tollefson et al. (2017)). (Cloud image credit: NASA, ESA, A. Simon (Goddard Space Flight Center), and M.H. Wong (University of California, Berkeley)).

Consequently, all RO experiments conducted by Juno are performed in two-way mode. In this configuration, a stable frequency reference signal is sent from the ground station in the X-band and converted on the spacecraft to other frequency bands. This method allows for two-band occultation analysis to mitigate potential ionospheric interference in the neutral atmosphere (Caruso et al., 2025; Hubbard et al., 1975, 1995). An additional challenge is ensuring correct antenna pointing. Unlike Cassini (Schinder et al., 2011), which adjusted the antenna dynamically during occultations, Juno's antenna pointing is fixed for the entire experiment, causing beam distortion and potential delays in signal acquisition during egress.

This study uses a two-way ray tracing technique, as described by Schinder et al. (2015) and Caruso et al. (2025). Data from the DSN Open-Loop Receiver is sampled without tracking at rates between 16 and 100 kHz. Frequency estimates are extracted using a Fast Fourier Transform with 0.1- or 0.25-s intervals, and mixed with reference frequencies to reconstruct the sky frequency for analysis. For experiments with rapidly changing signal dynamics from spacecraft motion or atmospheric refraction, a Phase-Lock Loop (PLL) was used for more accurate signal tracking (Buccino et al., 2018). While a well-tuned PLL offers superior noise rejection, it remains sensitive to residual dynamics and thermal noise. We apply a Savitzky–Golay filter to suppress outliers in the frequency data. For the RO analysis, the atmosphere is modeled as zonally symmetric and barotropic, implying that the atmosphere consists of equipotential surfaces of constant density, pressure, and potential. The gravitocentrifugal, potential is calculated as

$$U = \frac{GM}{r}\left[-1 + J_2P_2(\sin\theta)\left(\frac{a}{r}\right)^2 + J_4P_4(\sin\theta)\left(\frac{a}{r}\right)^4 + J_6P_6(\sin\theta)\left(\frac{a}{r}\right)^6\right] + Q, \quad (1)$$

where GM is Jupiter's gravitational parameter, r is the radius, J_n and P_n are the zonal harmonic coefficients and the associated Legendre polynomials respectively, θ is the planetocentric latitude, a is a reference radius and $Q = \int_0^l \omega^2 l' dl'$ represents the centrifugal component of the potential, where $l = r\cos\theta$ is the distance from the axis of rotation, and ω is the rotation rate, precomputed numerically using a wind model of Jupiter (Tollefson

et al., 2017). The winds influence the constant potential surfaces U (Galanti et al., 2023). Due to the barotropic assumption, these surfaces coincide with surfaces of constant density, refractive index n, and refractivity ($N = n - 1$). The gradient of refractivity determines the bending of rays as they traverse Jupiter's atmosphere.

The atmospheric structure is derived using the two-way ray tracing technique, tracing rays through the unknown atmosphere while iteratively optimizing to match the uplink and downlink signals. This process produces a layered model of the atmosphere with known constant refractivity gradients. Converting these gradients into temperature-pressure profiles requires knowledge of the atmospheric composition. The most recent Voyager reanalysis from Gupta et al. (2022) has already refined the Voyager occultation profiles (first shown in Lindal et al., 1981). The density profile is calculated using

$$\rho = N\frac{m_m}{\kappa}, \tag{2}$$

where m_m is the mean molecular mass and κ is the mean refractive volume, using the values for the composition from Gupta et al. (2022). The number density $\rho_n = N/\kappa$ is subsequently also used in the calculations. Next, the density is integrated assuming hydrostatic balance to yield the temperature,

$$T = T(U_0)\frac{\rho_n(U_o)}{\rho_n} + \frac{1}{k_B\rho_n}\int_U^{U_0}\rho dU. \tag{3}$$

Here k_B is the Boltzmann constant and U_0 is the potential level of reference at which the upper boundary condition $T(U_0)$ is enforced (Caruso et al., 2025). Finally, using the ideal gas law, the pressure is obtained from

$$p = k_B\rho_n T. \tag{4}$$

This process provides temperature-pressure profiles of Jupiter's atmosphere. The vertical resolution is limited by the diameter of the first Fresnel zone, $2\sqrt{\frac{\lambda d_t d_r}{d_t + d_r}}$, where λ is the transmitted wavelength, and d_t is the distance from the transmitter (Juno) to the tangent point and d_r is the distance from the tangent point to the receiver (Earth). Using the measured tangent-point distances for the Juno occultations, the average Fresnel diameters are: ~1.8 km on ingress and ~2.8 km on egress for X-band and ~0.95 km on ingress and ~1.6 km on egress for Ka-band, well below the atmospheric scale height (Karayel & Hinson, 1997) (accompanying Table in Supporting Information S1). A simple smoothing technique is applied to remove any residual noise from the profiles. It is essential to note that setting an upper boundary temperature at 1 mbar (for Jupiter between 145 and 175 K), from which integration begins, can influence the profile in the stratosphere. Given the need to assume an upper temperature boundary, the range of temperatures at 1 mbar measured by the CIRS instrument on Cassini (Fletcher et al., 2016) was adopted. The total error in the vertical profiles results from various sources, including trajectory inconsistencies, choice of wind profile, signal noise, and upper boundary selection, as is thoroughly discussed in Caruso et al. (2025). A detailed comparison of the grazing and non-grazing retrieved profiles with those presented in Caruso et al. (2025), illustrating how differences arise from the implementation of the methodology, is provided in Supporting Information S1 (Figures S1a and S1b).

2.2. Mid-IR Observations

To provide broader spatial and temporal context for the Juno RO measurements, we incorporate two complementary datasets: archival mid-infrared observations from Cassini/CIRS (Fletcher et al., 2016) and more recent ground-based data from TEXES on NASA's Infrared Telescope Facility (IRTF) (Lacy et al., 2002). The CIRS data were acquired during Cassini's 2000 flyby of Jupiter, while TEXES observations are ongoing and more closely aligned with the Juno occultations discussed here (Smirnova, 2025). Jupiter's atmospheric temperatures, gas composition, and aerosol opacity are mapped using mid-infrared spectra (5–20 μm) obtained with TEXES. For over a decade, TEXES has enabled routine monitoring of Jupiter's thermal structure through low-to medium-resolution observations. By targeting 8–10 specific wavenumber settings, these measurements capture key spectral features and provide a three-dimensional view of the atmosphere from the troposphere (0.6 bar) to the mid-stratosphere (1 mbar). Inversion methods for deriving temperature profiles from TEXES data are detailed in Fletcher et al. (2016), based on the December 2014 observations. Although full temperature retrievals are not

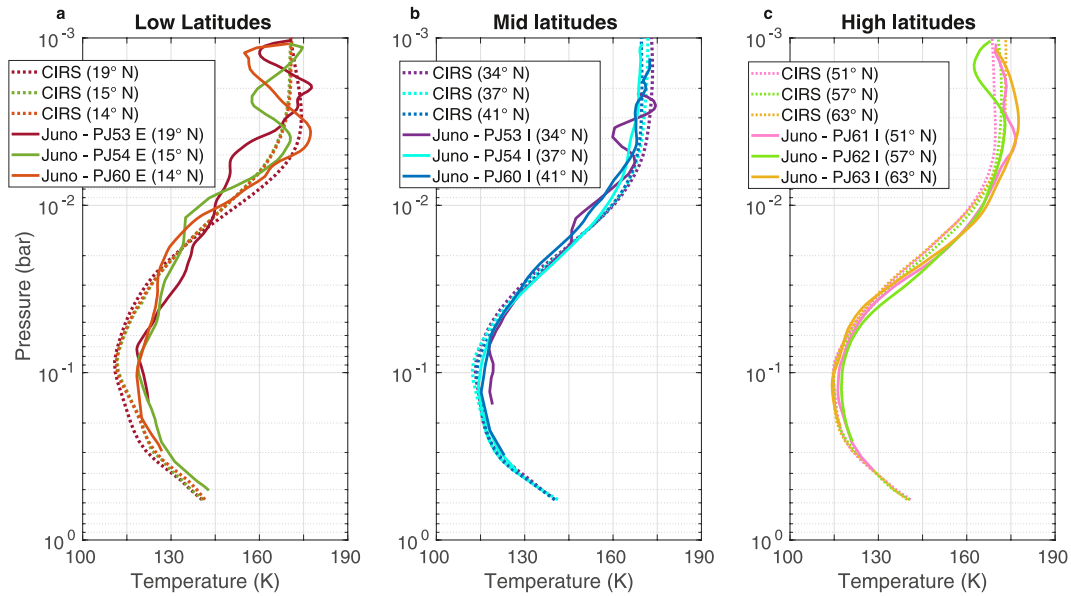

Figure 2. Temperature-pressure profiles of 9 radio occultations grouped into low (a), mid (b) and high (c) latitudinal sectors, shown against vertical profiles of CIRS measurements at same latitudes (Accompanying Table in Supporting Information S1). All latitudes refer to the top of the profile (at 1 mbar) and are planetocentric.

performed for every epoch, TEXES brightness temperature maps still offer valuable insights by approximating the kinetic temperature structure, and are well suited to complement the vertical profiles derived from Juno's radio occultations.

3. Temperature Retrieval

The analysis of radio occultations reveals distinct temperature–pressure profiles across different latitudes of Jupiter's atmosphere. These are presented in Figure 2, grouped into three latitudinal regions. All latitudes refer to the top of the profile (at 1 mbar) and are planetocentric, highlighting the latitudinal dependence of the vertical thermal structure. The PJ-53, PJ-54, and PJ-60 Egress occultations were conducted at low latitudes (14°, 15°, and 19°N), while PJ-53, PJ-54, and PJ-60 Ingress occurred at mid-latitudes (34°, 37°, and 41°N). High-latitude profiles come from PJ-61, PJ-62, and PJ-63 Ingress (54°, 57°, and 63°N). The PJ-53 Ingress profile is truncated at 2 mbar due to significant outliers caused by grazing geometry, where horizontal variations and signal degradation, especially in Ka band, impact retrieval quality (Caruso et al., 2025).

Each Juno RO profile is compared to a corresponding lower-resolution Cassini/CIRS temperature profile at the same latitude, extending to 600 mbar. For grazing occultations (PJ-53, PJ-54, PJ-60), ray paths span a broader latitude range (∼4.5°) than the typical ∼1.5° of nadir-like events. To mitigate this, CIRS profiles were sampled along the actual occultation latitude at each pressure level, enabling point-by-point comparison despite the spread. These profiles are based on Fletcher et al. (2016), using CIRS spectra at 2.5 cm^{-1} resolution over the 7–16 μm range. Stratospheric temperatures are constrained by methane emissions (1–10 mbar), the 80–250 mbar range by the hydrogen continuum, and the 300–600 mbar region by ammonia and CH_3D features. The inversions use a prior combining low-latitude averages from Fletcher et al. (2009) and Nixon et al. (2007), based on Galileo ASI data (Seiff et al., 1998) for the stratosphere and Galileo/Voyager data for the troposphere. Juno profiles are anchored to the CIRS-derived temperature at 1 mbar for each latitude.

All profiles, irrespective of latitude, show large-scale vertical temperature variations in the upper troposphere and lower stratosphere. At higher altitudes in the stratosphere, between 1 and 10 mbar, the highest temperatures are observed. From 10 mbar down to the tropopause at 100 mbar, temperatures decrease (minimum temperatures along the profile), before reversing and increasing again in the troposphere below the 100-mbar level. This warming trend continues downward, with the lowest measurement (200–500 mbar) depending on the depth at which the radio signal is lost during each experiment. This typical atmospheric profile is fully consistent with

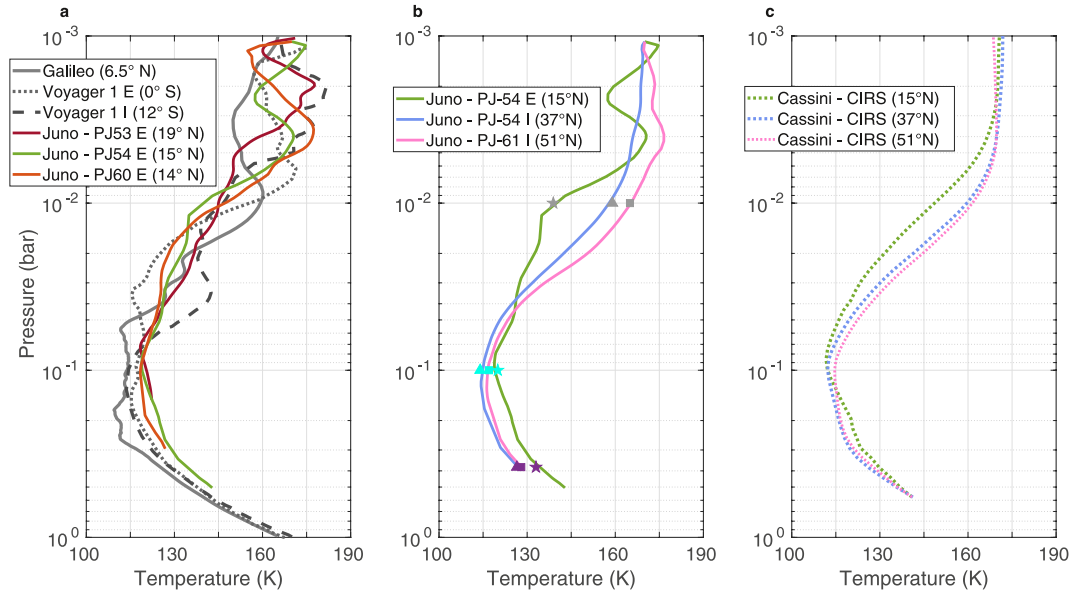

Figure 3. Panel (a) shows the lower latitudinal measurements of the atmosphere as represented by vertical profiles from the Galileo probe (Seiff et al., 1998), Voyager 1 (Gupta et al., 2022) and Juno measurements. In Panel (b) we show three representative Juno profiles at low, middle and high latitudes. Here we also indicate the pressure levels of 10 mbar (gray symbols), 100 mbar (light blue symbols) and 400 mbar (purple symbols), connecting the accompanying Texas Echelon Cross Echelle Spectrograph measurements of Figure 4 to the thermal structure. Panel (c) shows Cassini CIRS measurements at the same latitudes as the profiles in (b) specific for comparison.

previous observations (Fletcher, Kaspi et al., 2020; Fletcher, Orton et al., 2020; Gupta et al., 2022; Lindal et al., 1981). Each profile is accompanied by a pressure-dependent uncertainty, for which a detailed uncertainty analysis is provided in (Caruso et al., 2025). Here we describe the typical values for grazing and non-grazing occultations. For non-grazing events, the dominant source of uncertainty in the stratosphere (between 1 and 10 mbar) is the upper boundary condition, contributing up to ±10 K and diminishing steadily along the profile, with additional contributions from instrument noise, assumed wind profiles, and spacecraft position. These are smaller, around ± 2 K near 10 mbar, diminishing to ±1 K in the troposphere below 100 mbar, which is also the total average error at the bottom of non-grazing RO experiments. For grazing occultations (especially PJ-53), noise plays a larger role, with a broader envelope of approximately ±25 K at the top, decreasing to ±10 K near 10 mbar, and ±2 K in the troposphere below 100 mbar.

Focusing on smaller-scale latitudinal temperature variations, the key observation is the significant variability at lower latitudes (Figure 2a) compared to the more stable temperature-pressure profiles at mid (Figure 2b) and high (Figure 2c) latitudes. Profiles closer to the equator not only exhibit more turbulent structures but also show greater variation relative to each other.

While CIRS measurements are included for comparison in Figure 2, their vertical resolution is set by the contribution functions shown in Fletcher et al. (2016), and is a function of the density of the absorbers at a specific altitude and their resulting opacity, which means that CIRS has more difficulty capturing finer-scale variations compared to RO data. Nonetheless, Juno RO profiles show good agreement with CIRS data at mid and high latitudes (Fletcher et al., 2016). In contrast, at lower latitudes, the agreement is less pronounced between 10 and 100 mbar, where CIRS data had lower vertical resolution (smooth interpolation between mid-stratosphere and upper troposphere) but becomes more evident below the tropopause with the rise in temperature.

Next, we examine whether the temporal and spatial variability seen in the low-latitude region (Figure 2a) was also present in earlier RO measurements. Figure 3a shows profiles from Jupiter's lower latitudes, including data from the Galileo probe (Seiff et al., 1997, 1998) at 6.5°N, Voyager 1 ingress and egress profiles (Lindal et al., 1981) at 12°S and 0°, and the Juno measurements at 14°, 15°, and 19°N. RO profiles from Pioneer 10, Pioneer 11, and Voyager 2 are excluded due to their specific locations or lack of available data. These earlier measurements reveal notable temperature differences across missions, reinforcing the region's variability. Jupiter's equatorial

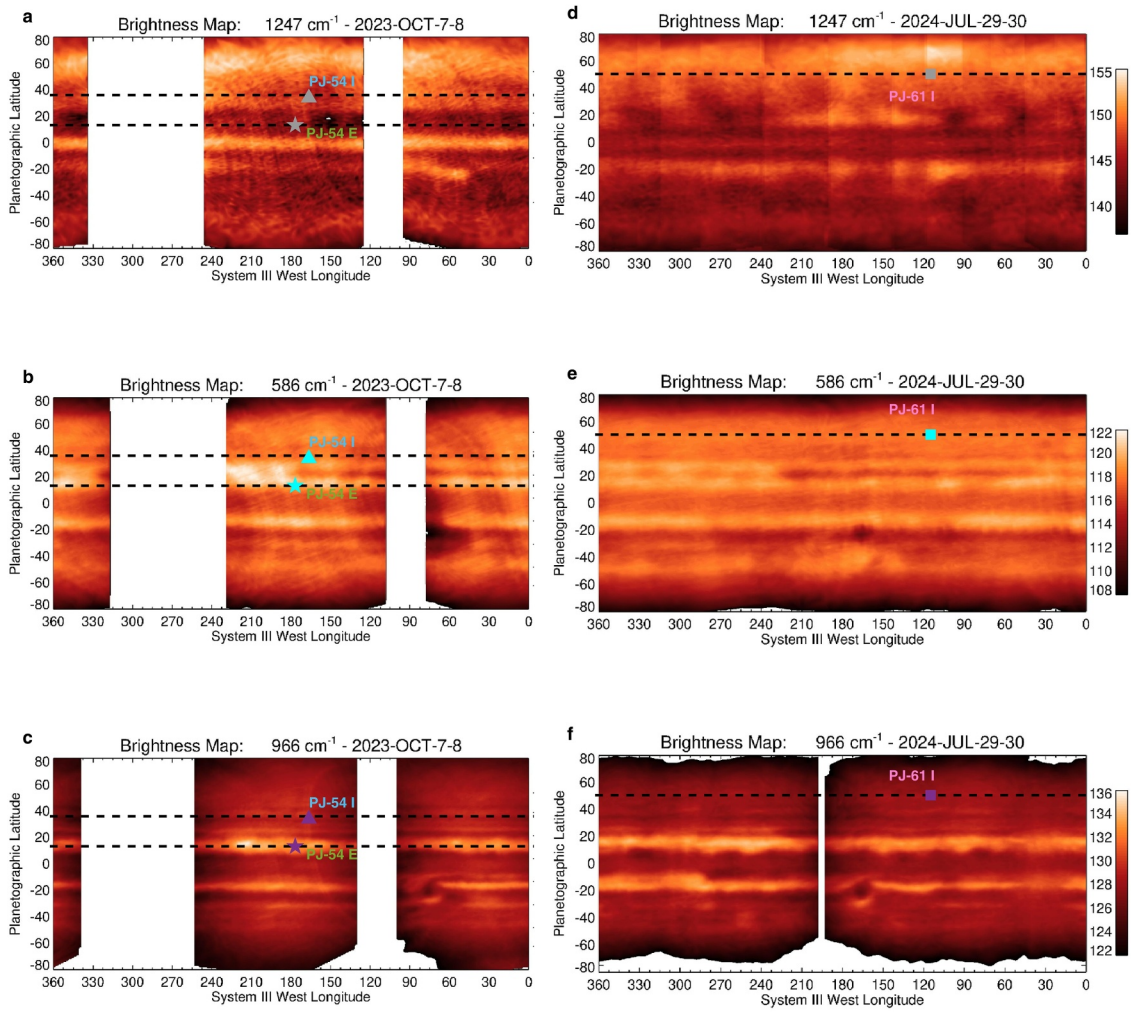

Figure 4. In the left column: Texas Echelon Cross Echelle Spectrograph Stratospheric (1,247 cm^{-1}) and tropospheric maps (586 cm^{-1} and 966 cm^{-1}) from October 2023, including path of radio occultation (RO) PJ-54 and in the right column the same maps for PJ-61 Ingress. The colorbar indicates brightness temperature in K. On the maps indicated with colored symbols are the latitudes and depths of the Juno radio occultations appearing in Figure 3b (Accompanying Table in Supporting Information S1).

stratospheric oscillation (JESO) features an off-equatorial structure in the North Equatorial Belt (NEB) that is in anti-phase with the quasi-quadrennial oscillation (QQO) near the equator. The QQO period is close to 4 years, though variable over time due to atmospheric disturbances (Antuñano et al., 2021; Leovy et al., 1991; Showman et al., 2020). This phase difference is seen in the oscillatory structures of Voyager 1 egress (equator) and ingress (mid-NEB), and may contribute to the vertical variability in the Juno profiles. While a clear downward-moving peak is hard to identify over the ∼1-year span, PJ-60 egress shows a possible oscillation signature near the tropopause, suggesting JESO influences temperatures over multi-year timescales (Antuñano et al., 2023; Orton et al., 2023).

Representative RO profiles from PJ-54 ingress and egress, and PJ-61 ingress, selected for their deep atmospheric coverage, are shown in Figure 3b. The 15°N profile, in the NEB (one of Jupiter's warmest tropospheric bands), shows cooler stratospheric and warmer tropospheric temperatures compared to profiles at 37°N and 51°N. Pressure levels at 10, 100, and 400 mbar are marked for comparison with the TEXES data in Figure 4. Figures 3b and 3c compare our results to CIRS observations at the same latitudes from 23 years earlier, further highlighting equatorial variability. The lower stratosphere is cooler at 15°N, while the troposphere is relatively warmer than at mid- and high-latitudes. Additional confirmation comes from recent ground-based TEXES measurements (Fletcher et al., 2016).

The TEXES maps, supporting the RO data, are displayed in Figure 4. The first column shows measurements from October 2023, coinciding with the PJ-54 occultation. The second column presents TEXES data from July 2024, nearly a year later, aligning with the PJ-61 occultation. Even though the date of the TEXES measurement is closer to the PJ-63 occultation, PJ-61 was selected for this comparison due to the depth of the RO measurement. We note that the warm equatorial band weakened in 2024, with TEXES data from late 2023 to mid-2024 showing a consistent cooling trend as the JESO shifted downward. Although full temperature retrievals were not performed for these maps, the brightness temperatures provide a useful proxy for kinetic temperatures, offering valuable context to support and interpret the RO profiles.

The stratospheric map at 1,247 cm^{-1} shows thermal contrasts around the 10 mbar level, while tropospheric maps at 586 cm^{-1} and 966 cm^{-1} indicate contrast at approximately 100 mbar (due to collision-induced absorption from hydrogen and helium) and 400 mbar (from a mix of temperatures, aerosols, and ammonia), respectively. These maps reveal that the PJ-54 ingress location (gray triangle) is warmer in the stratosphere than the PJ-54 egress location (gray star), which is expected as the latter is in a cooler, darker band at 10 mbar (Figure 4). This warm stratospheric region is thought to be consistently warmer than the same latitudes in the southern hemisphere (Antuñano et al., 2023), making comparisons with future southern occultations intriguing. Additionally, PJ-54 egress occurs within the NEB, where elevated tropospheric temperatures are expected at the 100 mbar (blue triangle) and 400 mbar (purple triangle) levels. For PJ-61, the comparison is less clear, but stratospheric temperatures are notably higher than at 15°N, as also seen in CIRS data.

Juno's RO also provide insights into Jupiter's atmospheric dynamics. They can be used to perform local wind shear calculations, offering perspective on the thermal structure and zonal winds above the cloud tops. We applied the thermal-wind equation $\frac{du}{dz} = -\frac{g}{fT}\frac{dT}{dy}$ to derive the wind shear in the region around the 21° jet, above the clouds. Here, f is the Coriolis parameter and $\frac{dT}{dy}$ is the meridional temperature gradient. We observe strong negative shear of about -0.6 ms^{-1} per km of height in the stratosphere near the 10 mbar level, and a weak positive shear of about 0.2 ms^{-1} per km of height at the tropopause and below. These measurements are consistent with previous wind shear calculations from CIRS and TEXES (Flasar et al., 2004; Fletcher et al., 2016; Read et al., 2006; Simon-Miller et al., 2006). As the mission evolves, and more radio occultations are available, more accurate measurements of the wind shear will be possible.

4. Discussion

The first year of radio occultations has yielded numerous high-resolution experiments of Jupiter's atmospheric thermal structure. RO experiments with Juno open a new era of opportunities by probing the relatively unexplored upper atmosphere with resolutions akin to descending a probe into the atmosphere. These analyses have enhanced our understanding of the thermal structure of Jupiter's stratosphere and upper troposphere. Our results show significantly larger vertical variability in the equatorial region than at higher latitudes, as seen in the PJ-54 egress occultation at 15°N, aligning with Jupiter's off-equatorial Equatorial Stratospheric Oscillation (JESO) region. Both Juno and CIRS data consistently show a colder stratosphere and warmer troposphere at 15°N compared to mid- and high latitudes. While CIRS measurements place the tropopause at a shallower pressure level than ROs, this may be due to their choice of prior for spectral inversions. Future reanalysis is needed to align CIRS data with Juno findings. Concurrent TEXES maps provide spatial context, confirming JESO activity and distinct temperature profiles at 15°N (Antuñano et al., 2021).

We observe small differences between the Juno and Voyager 1 RO profiles at lower latitudes. These discrepancies may result from slight differences in the latitudes of the occultation paths, or could reflect genuine temporal variability in Jupiter's atmosphere. Jupiter's thermal structure is known to exhibit variability on seasonal to multi-decadal timescales. For example, brightness temperature differences of 0.3–2.7 K in the 8.6–19.5 μm range have been reported between Voyager IRIS (1979) and Cassini CIRS (2000) observations (Antuñano et al., 2019), which may be due in part to instrumental differences but are also consistent with long-term atmospheric variability. Extended analyses over the past four decades (Antuñano et al., 2023; Orton et al., 2023; Simon-Miller et al., 2006) have shown cyclic thermal changes, including 4–5 K variations in the mid-latitude stratosphere and 2–3 K in the upper troposphere, as well as significant evolution in the structure of Jupiter's equatorial oscillation (Antuñano et al., 2021).

Atmospheric dynamics likely shape the temperature variability seen in Juno's RO profiles. Allison (1990) compared low-latitude Voyager 1 occultation profiles, which showed vertical oscillations, to a smoother high-latitude Voyager 2 profile. This contrast was taken as evidence that vertical wave propagation is inhibited at high latitudes, likely due to the trapping of large-scale equatorially confined disturbances, pointing to deeper dynamical processes below the occultation region. With Juno's broader latitude coverage, this interpretation can now be tested more robustly. Our observations support it: high-latitude profiles tend to be more vertically uniform, while low-latitude profiles often exhibit oscillatory features. This suggests that wave propagation remains latitude-dependent, with activity largely confined to lower latitudes.

These results underscore the value of spatially distributed, contemporaneous datasets for assessing latitudinal variability in wave activity. Long-term, multi-mission comparisons further illuminate Jupiter's vertical and horizontal dynamical structure. We also observe strong negative wind shear near 10 mbar and weak positive shear near the tropopause, consistent with previous CIRS and TEXES results (Flasar et al., 2004; Fletcher et al., 2016; Read et al., 2006; Simon-Miller et al., 2006). Future occultation experiments will help refine these trends.

Juno RO measurements reliably probe down to ∼0.5 bar. The upcoming JUICE mission, which will reach 1 bar and deeper, will provide key constraints on temperatures at depth, critical for interior modeling (Howard et al., 2023; Miguel & Vazan, 2023; Ziv et al., 2024). RO-derived temperature–pressure profiles will also support improved estimates of Jupiter's shape, as they are linked to the radius at each equipotential surface (Galanti et al., 2023; Helled et al., 2011).

This study provides the first high-resolution temperature measurements of Jupiter's atmosphere in over four decades. Importantly, we present a coherent view of the thermal structure of both the Jovian stratosphere and troposphere, based on three complementary datasets: Juno radio occultations, Cassini CIRS data, and ground-based TEXES measurements. Together, these observations improve our knowledge of Jupiter's atmospheric thermal structure and provide additional constraints for modeling its dynamic weather systems and interior processes.

Conflict of Interest

The authors declare no conflicts of interest relevant to this study.

Data Availability Statement

The data used to create the Juno RO temperature-pressure profiles, the CIRS-derived profiles, the Voyager 1 I and E profiles, the Galileo profile and the TEXES images (.jpg and.fits) can be found via Smirnova (2025). The Juno radio science data used in this research are publicly available through NASA's Planetary Data System via Buccino (2016). TEXES observations from October 2023 (2023B-049, PI G.S. Orton) and July 2024 (2024A-015, PI J. Harkett) were acquired by T.K. Greathouse using the IRTF at Mauna Kea (80HQTR24DA010), we recognize the significant cultural role within the indigenous Hawaiian community, and appreciate the opportunity to conduct our Jupiter observations from this revered site. The TEXES data are originally available via Fletcher (2024).

Acknowledgments
We acknowledge support by the Israeli Space Agency and the Helen Kimmel Center for Planetary Science at the Weizmann Institute. AC, LGC, MZ, and PT are grateful to the Italian Space Agency (ASI) for financial support through Agreement No. 2023-6-HH.0 in the context of ESA's JUICE mission, and Agreement No. 2022-16-HH.0, for ESA's BepiColombo and NASA's Juno radio science experiments. WBH, PGS, and SB were supported by NASA Contract NNM06AA75C from the Marshall Space Flight Center and the work of DB, GO, MP, RSP and SML was carried out at the Jet Propulsion Laboratory, California Institute of Technology, under a contract with the National Aeronautics and Space Administration (80NM0018D0004). LNF was supported by STFC Consolidated Grant reference ST/W00089X/1. We also want to thank J. Harkett and T.K. Greathouse for providing us with the TEXES data. For the purpose of open access, the author has applied a Creative Commons Attribution (CC BY) licence to the Author Accepted Manuscript version arising from this submission.

References

Allison, M. (1990). Planetary waves in Jupiter's equatorial atmosphere. *Icarus*, *83*(2), 282–307. https://doi.org/10.1016/0019-1035(90)90069-I

Antuñano, A., Cosentino, R. G., Fletcher, L. N., Simon, A. A., Greathouse, T. K., & Orton, G. S. (2021). Fluctuations in Jupiter's equatorial stratospheric oscillation. *Nature Astronomy*, *5*, 71–77. https://doi.org/10.1038/s41550-020-1165-5

Antuñano, A., Fletcher, L. N., Orton, G. S., Melin, H., Donnelly, P. T., Roman, M. T., et al. (2023). Jupiter's multi-year cycles of temperature and aerosol variability from ground-based mid-infrared imaging. *Journal of Geophysical Research: Planets*, *128*(12), e2022JE007693. https://doi.org/10.1029/2022je007693

Antuñano, A., Fletcher, L. N., Orton, G. S., Melin, H., Milan, S., Rogers, J., et al. (2019). Jupiter's atmospheric variability from long-term ground-based observations at 5μm. *The Astronomical Journal*, *158*(3), 130. https://doi.org/10.3847/1538-3881/ab2cd6

Antuñano, A., Fletcher, L. N., Orton, G. S., Melin, H., Rogers, J. H., Harrington, J., et al. (2018). Infrared characterization of Jupiter's equatorial disturbance cycle. *Geophysical Research Letters*, *45*(20), 10987–10995. https://doi.org/10.1029/2018gl080382

Bolton, S. J., Adriani, A., Adumitroaie, V., Allison, M., Anderson, J., Atreya, S., et al. (2017). Jupiter's interior and deep atmosphere: The initial pole-to-pole passes with the Juno spacecraft. *Science*, *356*(6340), 821–825. https://doi.org/10.1126/science.aal2108

Bolton, S. J., Lunine, J., Stevenson, D., Connerney, J. E. P., Levin, S., Owen, T. C., et al. (2017). The Juno mission. *Space Science Reviews*, *213*(1–4), 5–37. https://doi.org/10.1007/978-94-024-1560-5_2

Buccino, D. (2016). Juno Jupiter gravity science raw data set V1.0, JUNO-J-RSS-1-JUGR-V1.0, NASA planetary data system (PDS) [Dataset]. Retrieved from https://atmos.nmsu.edu/PDS/data/jnogrv_1001/

Buccino, D., Parisi, M., Gramigna, E., Casajus, L., Tortora, P., Zannoni, M., et al. (2022). Ganymede's ionosphere observed by a dual-frequency radio occultation with Juno. *Geophysical Research Letters*, *49*(23), e2022GL098420. https://doi.org/10.1029/2022gl098420

Buccino, D., Parisi, M., Kahan, D., Wilson, H., Yang, O., Barbinis, E., et al. (2023). Planning and execution of Juno radio occultation experiments at Jupiter. In *2023 IEEE aerospace conference* (pp. 1–10). https://doi.org/10.1109/AERO55745.2023.10115541

Buccino, D. R., Kahan, D. S., Yang, O., & Oudrhiri, K. (2018). Extraction of doppler observables from open-loop recordings for the Juno radio science investigation. In *2018 United States national committee of URSI national radio science meeting (USNC-URSI NRSM)* (pp. 1–2). IEEE

Caruso, A., Gomez Casajus, L., Smirnova, M., Buccino, D., Galanti, E., Hubbard, W. B., et al. (2025). Probing Jupiter's atmosphere through Juno Radio occultations: Methodology and initial observations. *Geophysical Research Letters*, *52*, e2024GL113231. https://doi.org/10.1029/2024GL113231

Coffin, D. A., Withers, P., Agiwal, O., Buccino, D., Parisi, M., Park, R. S., et al. (2025). Juno-derived electron density profiles of the high-latitude Jovian ionosphere. *Journal of Geophysical Research: Space Physics*, *130*(6), e2025JA033754. https://doi.org/10.1029/2025ja033754

Conrath, B. J., Flasar, F. M., Pirraglia, J. A., Gierasch, P. J., & Hunt, G. E. (1981). Thermal structure and dynamics of the Jovian atmosphere. II - Visible cloud features. *Journal of Geophysical Research*, *86*(A10), 8769–8775. https://doi.org/10.1029/ja086ia10p08769

Conrath, B. J., Gierasch, P. J., & Ustinov, E. A. (1998). Thermal structure and para hydrogen fraction on the outer planets from Voyager/IRIS measurements. *Icarus*, *135*(2), 501–517. https://doi.org/10.1006/icar.1998.6000

Flasar, F. M., Kunde, V. G., Achterberg, R. K., Conrath, B. J., Simon-Miller, A. A., Nixon, C. A., et al. (2004). An intense stratospheric jet on Jupiter. *Nature*, *427*(6970), 132–135. https://doi.org/10.1038/nature02142

Fletcher, L. (2024). leighfletcher/TEXES-Jupiter: TEXES Jupiter database [Dataset]. *Zenodo*. https://doi.org/10.5281/zenodo.13860951

Fletcher, L. N., Cavalié, T., Grassi, D., Hueso, R., Lara, L. M., Kaspi, Y., et al. (2023). Jupiter science enabled by ESA's Jupiter Icy Moons explorer. *Space Science Reviews*, *219*(7), 53. https://doi.org/10.1007/s11214-023-00996-6

Fletcher, L. N., Greathouse, T., Orton, G., Sinclair, J., Giles, R., Irwin, P., & Encrenaz, T. (2016). Mid-infrared mapping of Jupiter's temperatures, aerosol opacity and chemical distributions with IRTF/TEXES. *Icarus*, *278*, 128–161. https://doi.org/10.1016/j.icarus.2016.06.008

Fletcher, L. N., Kaspi, Y., Guillot, T., & Showman, A. P. (2020a). How well do we understand the belt/zone circulation of giant planet atmospheres? *Space Science Reviews*, *216*(2), 30. https://doi.org/10.1007/s11214-019-0631-9

Fletcher, L. N., Orton, G., Stallard, T., Baines, K., Sayanagi, K. M., Martin-Torres, F. J., et al. (2009). Jupiter atmospheric science in the next decade. In *AAS/division for planetary sciences meeting abstracts #41, volume 41 of AAS/division for planetary sciences meeting abstracts* (pp. 16–27).

Fletcher, L. N., Orton, G. S., Greathouse, T. K., Rogers, J. H., Zhang, Z., Oyafuso, F. A., et al. (2020). Jupiter's equatorial plumes and hot spots: Spectral mapping from Gemini/TEXES and Juno/MWR. *Journal of Geophysical Research: Planets*, *125*(8), e06399. https://doi.org/10.1029/2020je006399

Galanti, E., Kaspi, Y., & Guillot, T. (2023). The shape of Jupiter and Saturn based on atmospheric dynamics, radio occultations and gravity measurements. *Geophysical Research Letters*, *50*(6), e2022GL102321. https://doi.org/10.1029/2022gl102321

Guerlet, S., Spiga, A., Delattre, H., & Fouchet, T. (2020). Radiative-equilibrium model of Jupiter's atmosphere and application to estimating stratospheric circulations. *Icarus*, *351*, 113935. https://doi.org/10.1016/j.icarus.2020.113935

Gupta, P., Atreya, S. K., Steffes, P. G., Fletcher, L. N., Guillot, T., Allison, M. D., et al. (2022). Jupiter's temperature structure: A reassessment of the Voyager radio occultation measurements. *The Planetary Science Journal*, *3*(7), 159. https://doi.org/10.3847/psj/ac6956

Helled, R., Anderson, J. D., Podolak, M., & Schubert, G. (2011). Interior models of Uranus and Neptune. *The Astrophysical Journal*, *726*(1), 15. https://doi.org/10.1088/0004-637x/726/1/15

Hinson, D. P., Flasar, F. M., Kliore, A. J., Schinder, P. J., Twicken, J. D., & Herrera, R. G. (1997). Jupiter's ionosphere: Results from the first Galileo radio occultation experiment. *Geophysical Research Letters*, *24*(17), 2107–2110. https://doi.org/10.1029/97gl01608

Howard, S., Guillot, T., Bazot, M., Miguel, Y., Stevenson, D. J., Galanti, E., et al. (2023). Jupiter's interior from Juno: Equation-of-state uncertainties and dilute core extent. *Astronomy and Astrophysics*, *672*, A33. https://doi.org/10.1051/0004-6361/202245625

Hubbard, W., Haemmerle, V., Porco, C., Rieke, G., & Rieke, M. (1995). The occultation of SAO 78505 by Jupiter. *Icarus*, *113*(1), 103–109. https://doi.org/10.1006/icar.1995.1008

Hubbard, W. B., Slattery, W. L., & Devito, C. L. (1975). High zonal harmonics of rapidly rotating planets. *The Astrophysical Journal*, *199*, 504–516. https://doi.org/10.1086/153717

Ingersoll, A. P. (1976). Pioneer 10 and 11 observations and the dynamics of Jupiter's atmosphere. *Icarus*, *29*(2), 245–252. https://doi.org/10.1016/0019-1035(76)90052-x

Ingersoll, A. P., & Cuong, P. G. (1981). Numerical model of long-lived Jovian vortices. *Journal of the Atmospheric Sciences*, *38*(10), 2067–2076. https://doi.org/10.1175/1520-0469(1981)038<2067:nmollj>2.0.co;2

Karayel, E. T., & Hinson, D. P. (1997). Sub-fresnel-scale vertical resolution in atmospheric profiles from radio occultation. *Radio Science*, *32*(2), 411–423. https://doi.org/10.1029/96rs03212

Kaspi, Y., Galanti, E., Hubbard, W. B., Stevenson, D. J., Bolton, S. J., Iess, L., et al. (2018). Jupiter's atmospheric jet streams extend thousands of kilometres deep. *Nature*, *555*(7695), 223–226. https://doi.org/10.1038/nature25793

Kaspi, Y., Galanti, E., Park, R. S., Duer, K., Gavriel, N., Durante, D., et al. (2023). Observational evidence for cylindrically oriented zonal flows on Jupiter. *Nature Astronomy*, *7*(12), 1463–1472. https://doi.org/10.1038/s41550-023-02077-8

Kliore, A. J., Woiceshyn, P. M., & Hubbard, W. B. (1976). Temperature of the atmosphere of Jupiter from pioneer 10/11 radio occultations. *Geophysical Research Letters*, *3*(3), 113–116. https://doi.org/10.1029/gl003i003p00113

Lacy, J. H., Richter, M. J., Greathouse, T. K., Jaffe, D. T., & Zhu, Q. (2002). TEXES: A sensitive high-resolution grating spectrograph for the mid-infrared. *Publications of the Astronomical Society of the Pacific*, *114*(792), 153–168. https://doi.org/10.1086/338730

Leovy, C., Friedson, A., & Orton, G. (1991). The quasiquadrennial oscillation of Jupiter's equatorial stratosphere. *Nature*, *354*(6352), 380–382. https://doi.org/10.1038/354380a0

Limaye, S. S., Revercomb, H. E., Sromovsky, L. A., Krauss, R. J., Santek, D. A., Suomi, V. E., et al. (1982). Jovian winds from Voyager 2. I: Zonal mean circulation. *Journal of the Atmospheric Sciences*, *39*(7), 1413–1432. https://doi.org/10.1175/1520-0469(1982)039<1413:jwfvpi>2.0.co;2

Lindal, G. F., Wood, G. E., Levy, G. S., Anderson, J. D., Sweetnam, D. N., Hotz, H. B., et al. (1981). The atmosphere of Jupiter: An analysis of the Voyager radio occultation measurements. *Journal of Geophysical Research*, *86*(A15), 8721–8727. https://doi.org/10.1029/ja086ia10p08721

Miguel, Y., & Vazan, A. (2023). Interior and evolution of the giant planets. *Remote Sensing*, *15*(3), 681. https://doi.org/10.3390/rs15030681

Nixon, C. A., Achterberg, R. K., Conrath, B. J., Irwin, P. G. J., Teanby, N. A., Fouchet, T., et al. (2007). Meridional variations of stratospheric temperatures and hydrocarbons on Saturn after one Saturn year of Cassini observations. *Icarus*, *188*(1), 47–71. https://doi.org/10.1016/j.icarus.2006.11.016

Orton, G. S., Antuñano, A., Fletcher, L. N., Sinclair, J. A., Momary, T. W., Fujiyoshi, T., et al. (2023). Unexpected long-term variability in Jupiter's tropospheric temperatures. *Nature Astronomy*, *7*, 190–197. https://doi.org/10.1038/s41550-022-01839-0

Orton, G. S., Fisher, B. M., Baines, K. H., Stewart, S. T., Friedson, A. J., Ortiz, J. L., et al. (1998). Characteristics of the Galileo probe entry site from Earth-based remote sensing observations. *Journal of Geophysical Research*, *103*(E10), 22791–22814. https://doi.org/10.1029/98je02380

Parisi, M., Caruso, A., Buccino, D., Gramigna, E., Withers, P., Casajus, L., et al. (2023). Radio occultation measurements of Europa's ionosphere from Juno's close flyby. *Geophysical Research Letters*, *50*(22), e2023GL106637. https://doi.org/10.1029/2023gl106637

Read, P. L., Gierasch, P. J., Conrath, B. J., Simon-Miller, A., Fouchet, T., & Yamazaki, Y. H. (2006). Mapping potential-vorticity dynamics on Jupiter. I: Zonal-mean circulation from Cassini and Voyager 1 data. *Quarterly Journal of the Royal Meteorological Society*, *132*(618), 1577–1603. https://doi.org/10.1256/qj.05.34

Sánchez-Lavega, A., Sromovsky, L. A., Showman, A. P., Del Genio, A. D., Young, R. M., Hueso, R., et al. (2019). *Zonal jets: Phenomenology, genesis, and physics* (1 edition, pp. 72–103). Cambridge University Press. https://doi.org/10.1017/9781107358225.004

Schinder, P., Flasar, F. M., Marouf, E., French, R. G., Anabtawi, A., Barbinis, E., & Kliore, A. (2015). A numerical technique for two way radio occultations by oblate axisymmetric atmospheres with zonal winds. *Radio Science*, *50*(7), 712–727. https://doi.org/10.1002/2015rs005690

Schinder, P. J., Flasar, F. M., Marouf, E. A., French, R. G., McGhee, C. A., Kliore, A. J., et al. (2011). Saturn's equatorial oscillation: Evidence of descending thermal structure from Cassini radio occultations. *Geophysical Research Letters*, *38*(8), L08205. https://doi.org/10.1029/2011gl047191

Seiff, A., Kirk, D. B., Knight, T. C. D., Young, L. A., Milos, F. S., Venkatapathy, E., et al. (1997). Thermal structure of Jupiter's upper atmosphere derived from the Galileo probe. *Science*, *276*(5309), 102–104. https://doi.org/10.1126/science.276.5309.102

Seiff, A., Kirk, D. B., Knight, T. C. D., Young, R. E., Mihalov, J. D., Young, L. A., et al. (1998). Thermal structure of Jupiter's atmosphere near the edge of a 5-μm hot spot in the north equatorial belt. *Journal of Geophysical Research: Planets*, *103*(E10), 22857–22889. https://doi.org/10.1029/98je01766

Showman, A. P., Tan, X., & Zhang, X. (2020). Atmospheric dynamics of hot giant planets and brown dwarfs. *Space Science Reviews*, *216*(8), 116. https://doi.org/10.1007/s11214-020-00758-8

Simon, A. A., Wong, M. H., & Orton, G. S. (2015). First results from the Hubble OPAL program: Jupiter in 2015. *The Astrophysical Journal*, *812*(1), 55. https://doi.org/10.1088/0004-637x/812/1/55

Simon-Miller, A. A., Conrath, B. J., Gierasch, P. J., Orton, G. S., Achterberg, R. K., Flasar, F. M., et al. (2006). Jupiter's atmospheric temperatures: From Voyager IRIS to Cassini CIRS. *Icarus*, *180*(1), 98–112. https://doi.org/10.1016/j.icarus.2005.07.019

Simon-Miller, A. A., Orton, G. S., & Irwin, P. G. J. (2004). *Jupiter's atmospheric structure, composition and dynamics* (pp. 129–158). Cambridge University Press.

Sinclair, J. A., Orton, G. S., Greathouse, T. K., Fletcher, L. N., Moses, J. I., Hue, V., et al. (2017). Jupiter's auroral-related stratospheric heating and chemistry I: Analysis of Voyager-IRIS and Cassini-CIRS spectra. *Icarus*, *292*, 182–207. https://doi.org/10.1016/j.icarus.2016.12.033

Smirnova, M. (2025). Juno P-T profiles for PJ53-PJ63 [Dataset]. *Harvard Dataverse*. https://dataverse.harvard.edu/dataset.xhtml?persistentId=doi:10.7910/DVN/LKMDJR

Tollefson, J., Wong, M. H., de Pater, I., Simon, A. A., Orton, G. S., Rogers, J. H., et al. (2017). Changes in Jupiter's zonal wind profile preceding and during the Juno mission. *Icarus*, *296*, 163–178. https://doi.org/10.1016/j.icarus.2017.06.007

Ziv, M., Galanti, E., Sheffer, A., Howard, S., Guillot, T., & Kaspi, Y. (2024). NeuralCMS: A deep learning approach to study Jupiter's interior. *Astronomy & Astrophysics*, *686*, L7. https://doi.org/10.1051/0004-6361/202450223